Research article

Spectral, NBO, NLO, NCI, aromaticity and charge transfer analyses of anthracene-9,10-dicarboxaldehyde by DFT

J. Jebasingh Kores [a,1], I. Antony Danish [b,1], T. Sasitha [c,1], J. Gershom Stuart [c,1], E. Jimla Pushpam [c,1], J. Winfred Jebaraj [c,*,1]

[a] Department of Physics, Pope's College (Autonomous), Sawyerpuram, 628251, Tamilnadu, India
[b] Department of Chemistry, Sadakathullah Appa College (Autonomous), Tirunelveli, 627011, Tamilnadu, India
[c] Department of Chemistry, St. John's College, Tirunelveli, 627002, Tamilnadu, India

ABSTRACT

Anthracene-9,10-dicarboxaldehyde (ADCA) is a polynuclear aromatic compound that has a planar structure with double bonds which are in conjugation. The molecule is subjected to theoretical investigation with DFT/B3LYP/6-311++G(d,p) basis set to find out the electronic structural properties and stability. Theoretical and experimental vibrational analyses are carried out. NBO studies predict that the molecule has high stability. NCI interaction studies reveal that Van der Waals force and steric effect are seen in the molecule. A shaded surface map with a projection of LOL analysis pointed out that electron depletion area is seen in this molecule. The tunnelling current is more in the boundary rings than the central ring. It is docked with the protein 4COF and the binding energy is found to be -6.6 kcal/mol. Electrons excitation analysis is performed and found that local excitation takes place for the lowest five excitations. The aromaticity of the molecule is also thoroughly investigated.

1. Introduction

Poly-nuclear aromatic compounds like anthracene are having a π conjugated electron system which has a great impact in many research areas like material science [1, 2]. The organic π electron systems have attracted great interest from both the scientific communities and industrialists on the basis of the potential applications as active elements in LED (Light-emitting electrode). The distribution of electron clouds on the aromatic moiety determines the optical and electro-physical properties. Ionization potential and electron affinity are always related to this kind of charge carriers. The mobility of the charge from one place to another is a key factor for the development of new organic optoelectronic material or devices. Normally anthracene and its derivatives have applications in organic electroluminescence investigations [3, 4, 5] and molecule conductivity studies [6]. The rich π conjugated system has a rigid planar structure.

The arrival of computational practices assists to predict the properties of molecules and to explore the chemical dependences. Usually DFT approach can give more accurate results than semi empirical methods [7]. This molecule has three rings, i.e., two terminals and one centre ring

with electron withdrawing substitution at the two corners of it. So it is decided to check how the aromaticity is varied? Properties like electronic structure, NBO (Natural Bond Orbital), NLO (Non Linear Optical), ESP (Electrostatic Potential), Frontier energy gap, Mulliken charge prediction, and theoretical spectral analysis, etc., are useful to interpret about a molecule completely. But unfortunately there is no such work has been done on this molecule. Hence it is decided to explore the properties by DFT and wave function analysis for the structurally important molecule. DFT investigation of anthracene-9,10-dicarboxaldehyde is carried out to investigate all the above said properties clearly. Since the molecule is a planar poly-nuclear ring system, the stability is expected to be very much. So we tried to identify which parameters are helpful to enhance the stability of this molecule. A thorough NBO study is carried out to know about the stability of the molecule. Wave function analyses which furnish more clarity about the structural properties like, NCI (Non Covalent Interaction), Shaded surface map determination, Hole-electron excitation, aromaticity determination, etc., are carried out.

The molecule under investigation is checked with PASS online tool to have an idea about the choice of proteins to bind. Interestingly the results suggested that this molecule can be docked well with around 200

---

proteins of various domains. From the results, it is found that this molecule under investigation can be used for phobia disorders. The human protein 4COF is related to this disease so it is decided to extend for molecular docking. The docking pattern of the target molecule with 4COF protein is investigated by PyRx tool and viewed by PyMOL programme.

2. Computational details

The gas-phase molecular geometry is optimized in the neutral state with the help of DFT using the B3LYP functionals. Becke's three-parameter hybrid exchange functional [8] combined with the Lee-Yang-Parr correlation functional basis set [9] with the diffuse function namely 6-311++G basis is implemented in Gaussian 16 package [10]. A valence double zeta set augmented with d polarisation function with s and p diffusion functions for each atom except for hydrogen is also included.

Basis sets with diffuse functions are important for systems where electrons are relatively far away from the nucleus and systems with low ionization potentials and so on. Unrestricted B3LYP formalism is used to carry out all the calculations. Recently DFT has appeared as a steadfast standard method for the theoretical research of geometrical and electronic properties like ionization potential, electronic excitation spectrum, etc., They have high accuracy for the wide range of the systems.

Multiwfn 3.8 tool is used to calculate NCI, shaded surface map, hole electron transfer, aromaticity, and simulated STM (Scanning Tunneling Microscope) deeply. PyRx and PyMOL tools are used to investigate the docking studies.

3. Experimental details

The FT-IR spectrum for the molecule is recorded in the 4000–400 cm^{-1} region with a Nicolet 1S5R FT-IR spectrometer using KBr pellets (AR) with diamond crystal plate. The UV-Visible spectrum is recorded by double beam UH-5300 spectrophotometer by dissolving 0.5 mg of the sample in 10 ml of absolute ethanol.

4. Results and discussion

4.1. Electronic structure determination

The molecule, anthracene-9,10-dicarboxaldehyde (ADCA) is optimized to obtain the fully converged structure. The convergence and full optimization are confirmed by GaussSum 3.0 tool. The absence of imaginary frequencies determined by Gaussian 16W tool also reveals that the molecule is fully optimized. The investigated molecule has 28 atoms and 122 electrons. It is found to be neutral and singlet in nature. The 2D and optimized 3D structures of the target molecule are shown in Figure 1 (a) and (b) respectively.
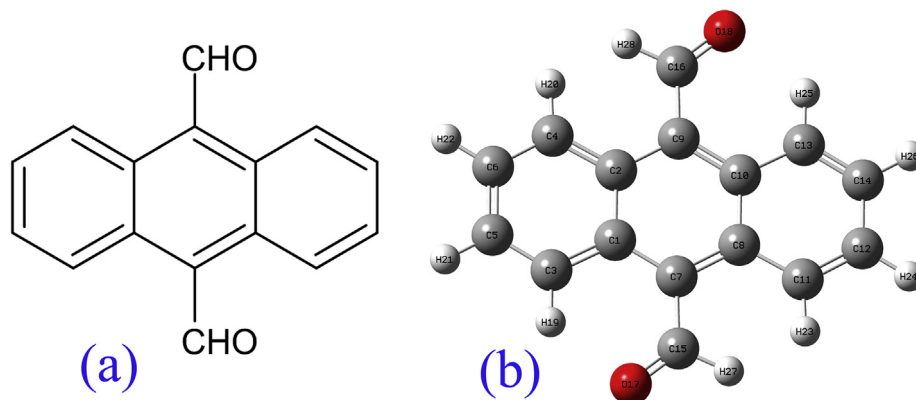
The atom numbering list generated by the Gaussian 16W software is listed in Table 1. The bond angle, bond distance, and dihedral angles for the optimized structure are determined by the DFT/B3LYP/6-311++G(d,p) basis set in the gaseous phase and listed in Table S1 (Supplementary Table 1). Trotter investigated the crystal structure of 9-anthraldehyde. The bond length and bond angle results are compared with the above results and found good [11]. Byru *et.al.,* has published a DFT work on the derivative of anthracene-9-carboxaldehyde, in which they specified the electronic structural properties along with XRD data. The measured values of the target molecule are in good agreement with the previous literature reports [12, 13, 14]. The average C–H bond length in anthracene molecule is estimated as 1.08 Å theoretically. The shortest C–H bond length of 1.076 Å is observed at 3C–19H and 13C–25H respectively. The longest bond of 1.492 Å is observed at 7C–15C and 9C–16C respectively. Two aldehyde carbons are attached to the aromatic ring. The calculated average bond angles between CCC are found to be 120.3° which are in good agreement with the reported experimental value of 120.9°. Likewise, the average bond angle between CCH is found to be 118.8°. The bond angle between CCH of aldehyde groups [(7C–15C–27H) and (9C–16C–28H)] are found to be 114.9° respectively. The angle between the CCO of aldehyde groups (9C–16C–18O) and (7C–15C–17O) are found to be 127.7° respectively.

4.2. Mulliken charge analysis

Mulliken charge for the target molecule is calculated at the same level of the basis set and is given in Table 2 and the plot generated is shown in Figure 2. From Table 2 and Figure 2, it is clear that the two oxygen atoms 17O and 18O are having almost the same charge (−0.215 a.u.). 1C, 2C, 7C, 8C, 9C, 10C are having positive charges and remaining carbon atoms are possessing negative charges.

1C is having greater charge of 0.8063 a.u. while the 4C is having the least charge of -0.7181 a.u. All the hydrogen atoms are having a positive charge. Among these 27H and 28H hydrogen atoms are having 0.1575 a.u. each since they are attached with carbonyl carbons. 21H and 26H atoms are having the charge of 0.1779 a.u. each respectively.

Table 1. The atom numbering list of ADCA.

1	2	3	4	5	6	7
C	C	C	C	C	C	C
8	9	10	11	12	13	14
C	C	C	C	C	C	C
15	16	17	18	19	20	21
C	C	O	O	H	H	H
22	23	24	25	26	27	28
H	H	H	H	H	H	H

Figure 1. (a) The 2D and (b) optimized 3D structures of ADCA.

Table 2. Mulliken charge of ADCA by B3LYP/6-311++G(d,p) method.

Atom	Charge (a.u.)	Atom	Charge (a.u.)
1C	0.8063	15C	-0.4298
2C	0.6310	16C	-0.4300
3C	-0.6784	17O	-0.2158
4C	-0.7181	18O	-0.2159
5C	-0.4100	19H	0.1885
6C	-0.3066	20H	0.0435
7C	0.5712	21H	0.1779
8C	0.6310	22H	0.1827
9C	0.5714	23H	0.0436
10C	0.8063	24H	0.1828
11C	-0.7180	25H	0.1885
12C	-0.3067	26H	0.1779
13C	-0.6782	27H	0.1575
14C	-0.4100	28H	0.1575

Table 3. Chemical reactivity parameters of ADCA at B3LYP/6-311++G(d,p) level.

S. No	Physical parameter	Charge (eV)
1	HOMO	-6.3003
2	LUMO	-3.4989
3	Energy gap (ΔE)	2.8014
4	Ionization potential (I)	6.3003
5	Electron affinity (A)	3.4989
6	Electronegativity (χ)	4.8996
7	Chemical hardness (η)	1.4007
8	Global softness (S)	0.7139
9	Chemical potential (μ)	-4.8996
10	Electrophilicity index (ω)	8.5693
11	Net electrophilicity ($\Delta\omega^{\pm}$)	-4.8997
12	Electron donating capability (ω^{-})	11.1942
13	Electron accepting capability (ω^{+})	6.2945
14	Additional electronic charge (ΔN_{max})	3.4979

4.3. Chemical reactivity

Density functional theory is a very useful framework for the study of chemical reactivity. Four decades ago DFT theory of chemical reactivity has been born. It provides the electronic structure of the chemical species [15]. Using HOMO and LUMO values the chemical reactivity parameters are calculated for ADCA using DFT with B3LYP/6-311++G(d,p) level of theory, and the values are listed in Table 3. The HOMO and LUMO are seen on overall molecule and exposed in Figure 3.

Electron affinity and ionization potential: Electron affinity (A) and ionization potential (I) measure the ability of chemical species to accept and donate one electron (Eqs. (1) and (2)). They are defined as,

$$A = -E_{LUMO} \tag{1}$$

$$I = -E_{HOMO} \tag{2}$$

E_{HOMO} and E_{LUMO} are the energies of highest occupied and lowest unoccupied molecular orbitals respectively.

Electro negativity and chemical potential: Electronegativity (χ) is one of the most used chemical concepts, a tendency of an atom or group that attracts an electron towards itself (eqn.3). It is the minus of chemical potential (μ). According to Mulliken [16, 17] it is defined as,

$$\chi = \frac{I + A}{2} \tag{3}$$

Using Koopman's theorem [16, 17, 18], the electron affinity and ionization potential can be replaced by the lowest unoccupied molecular orbital (LUMO) energy and highest occupied molecular orbital (HOMO) energy respectively (eqn.4).

$$\chi = -\mu = -\frac{E_{HOMO} + E_{LUMO}}{2} \tag{4}$$

Global hardness and softness: Global hardness (η) is equal to the energy difference between the occupied and unoccupied molecular orbitals (eqn.5). It is related to another molecular property global softness (S) (eqn.6). It is a reciprocal of hardness [17].

$$\eta = \frac{E_{LUMO} - E_{HOMO}}{2} \tag{5}$$

$$s = \frac{1}{\eta} \tag{6}$$

Electrophilicity and net electrophilicity: The ability of an electrophile to accept electrons from the nucleophile is called electrophilicity (eqn.7).
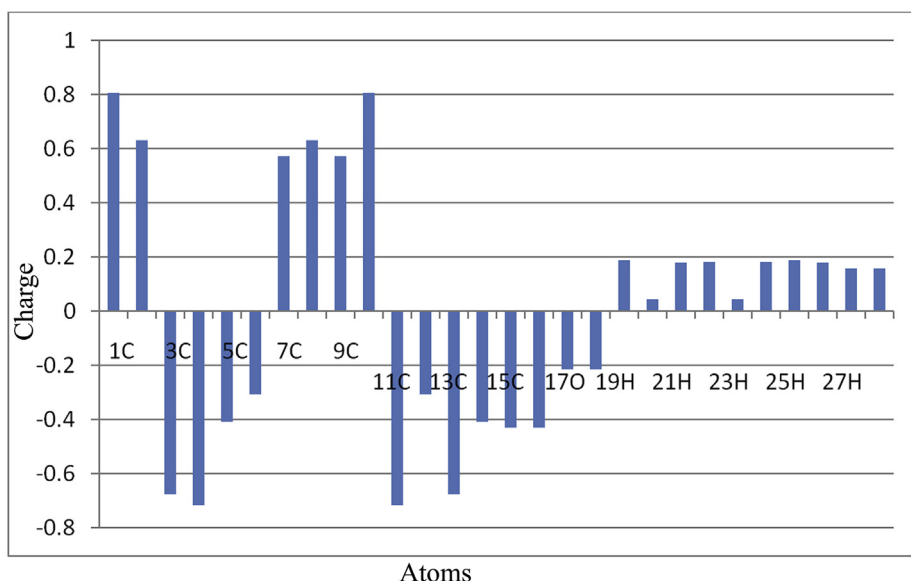
Figure 2. Mulliken charge plot of ADCA by B3LYP/6-311++G(d,p) method.
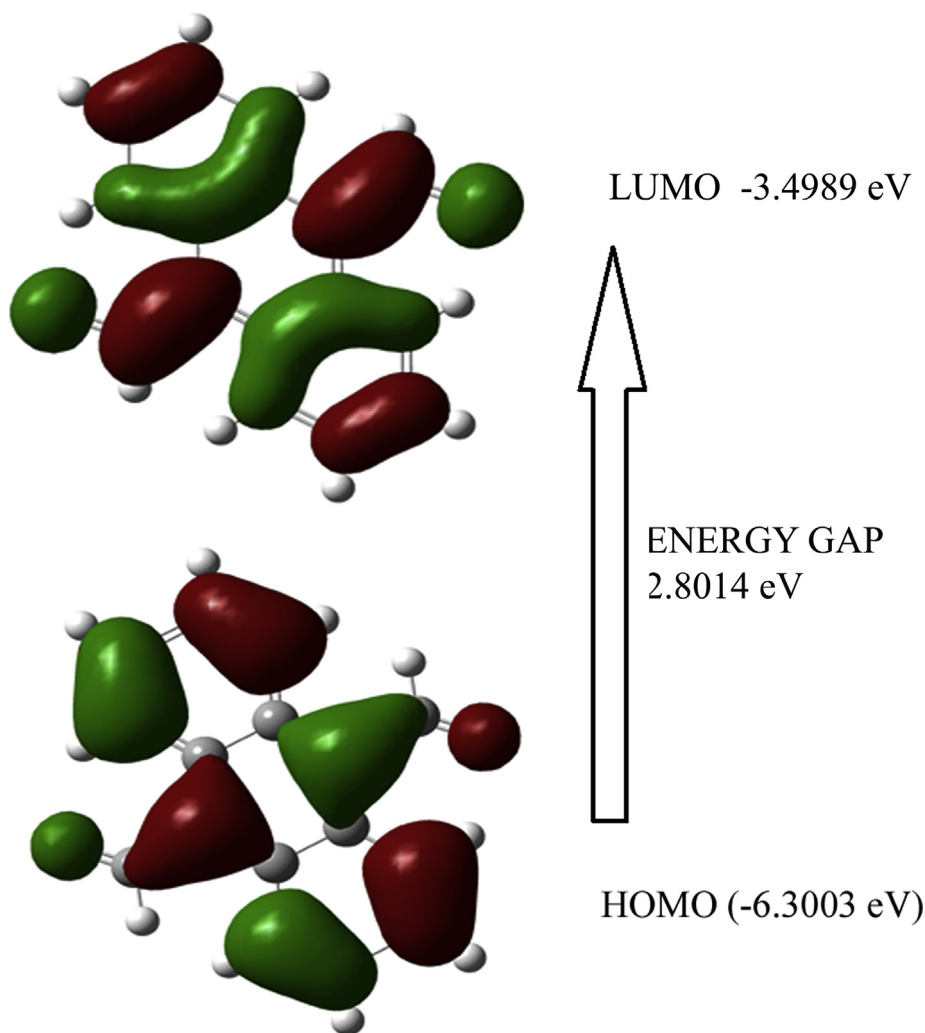
Figure 3. HOMO – LUMO of ADCA

In DFT, electrophilicity has been calculated by both chemical potential and hardness [19, 20].

$$\omega = \frac{\mu^2}{2\eta} \tag{7}$$

Using electron-accepting (ω^+) and electron-donating (ω^-) powers, net electrophilicity ($\Delta\omega^\pm$) (eqn.8) have been proposed [21].

$$\Delta\omega^\pm = \omega^+ - (\omega^-) \tag{8}$$

where

$$\omega^- = \frac{(3I + A)^2}{16(I - A)} \tag{9}$$

$$\omega^+ = \frac{(I + 3A)^2}{16(I - A)} \tag{10}$$

The additional electronic charge is defined as (eqn.11)

$$\Delta N_{max} = \frac{-\mu}{\eta} \tag{11}$$

The energy difference between HOMO and LUMO of ADCA is 2.8014 eV. So this molecule can be a stable molecule. The global hardness, softness, chemical potential, electronegativity, and electrophilicity index

of ADCA are found to be 1.4007, 0.7139, -4.8996, 4.8996, and 8.5692 eV respectively.

4.4. Molecular electrostatic potential (ESP) analysis

Molecular electrostatic potential of a molecule gives information about the properties like molecular size, dipole moment, shape, electronic density, hydrogen bonding interactions, and chemical reactivity etc., [22]. In molecular electrostatic potential, the surfaces are represented in red, blue, light blue, yellow, and green colors. The red colour represents the electron-rich (partially negative charge) area whereas the blue colour represents the electron poor (partially positive charge) locations. Light blue colour represents slightly electron-deficient region while the yellow colour represents a slightly electron-rich domain. The green colour represents a neutral charge location [23]. The electrostatic potential map for the title molecule is investigated by B3LYP/6-311++G(d,p) method and the electrostatic potential map with different colour representation is shown in Figure 4 (a). The region of red colour (electron-rich) is located around the oxygen atoms of the two aldehyde groups in which electrophilic attack is possible. Blue colour region (electron-poor) region is spread all over the molecule around hydrogen atoms which is prone to nucleophilic attack. The contour map of the investigated molecule is also analysed and shown in Figure 4 (b). From the map it is clear that the contour map spreads through all the atoms.

4.5. Non linear optical effect

The dipole moment, mean polarizability and first-order hyper-polarizability of the title compound is calculated by DFT/B3LYP/6-311++G(d,p) level of theory based on finite field approach. The first order hyperpolarizability is a third rank tensor that can be described by the $3 \times 3 \times 3$ matrix. Due to Kleinman symmetry [24] the 27 component of the 3D matrix can be reduced to 10 components.

The β components are defined as the coefficient in the Taylor series expansion (eqn.12) of the energy in the external electric field, which is weak and homogenous. This expansion is as follows

$$E = E^0 - \mu_\alpha F_\alpha - \frac{1}{2}\alpha_{\alpha\beta}F_\alpha F_\beta - \frac{1}{6}\beta_{\alpha\beta\gamma}F_\alpha F_\beta F_\gamma + \dots \quad (12)$$

where E^0 is the energy of the unperturbed molecules, μ_α, $\alpha_{\alpha\beta}$ and $\beta_{\alpha\beta\gamma}$ are the component of the dipole moment, polarizability and first-order hyperpolarizability respectively. Using x, y, z components the dipole moment, polarizability and hyperpolarizability are defined as follows (Eqs. (13), (14), (15), and (16)) [25, 26],

$$\mu = \sqrt{\mu_x^2 + \mu_y^2 + \mu_z^2} \quad (13)$$

$$\alpha = \frac{\alpha_{xx} + \alpha_{yy} + \alpha_{zz}}{3} \quad (14)$$

$$\Delta\alpha = \frac{1}{\sqrt{2}}\sqrt{\left(\alpha_{xx} - \alpha_{yy}\right)^2 + \left(\alpha_{yy} - \alpha_{zz}\right)^2 + \left(\alpha_{zz} - \alpha_{xx}\right)^2 + 6\alpha_{xx}^2} \quad (15)$$

$$\beta_{tot} = \sqrt{\left(\beta_x\right)^2 + \left(\beta_y\right)^2 + \left(\beta_z\right)^2} \quad (16)$$

where,

$$\beta_x = \beta_{xxx} + \beta_{xyy} + \beta_{xzz}$$

$$\beta_y = \beta_{yyy} + \beta_{yzz} + \beta_{yxx}$$

$$\beta_z = \beta_{zzz} + \beta_{zxx} + \beta_{zyy}$$

The polarizability and first-order hyper polarizability values of the Gaussian 16W output in atomic units, and the calculated values are converted into electrostatic units (For α, 1 a.u. = 0.1482×10^{-24} e.s.u.; for β, 1 a.u. = 8.6391×10^{-30} e.s.u.) [27]. They are shown in Table 4. As seen in Table 4, the calculated dipole moment, polarizability, anisotropy of polarizability and first-order hyperpolarizability of the title molecule are found to be 0.3621 Debye, 31.7134 x 10^{-24} and 0.8989 x 10^{-30} e.s.u. respectively.

Table 4. Dipole moment, polarizability and hyper polarizability of the target molecule determined by DFT method using the basis set B3LYP/6-311++G(d,p).

Parameters	B3LYP/6-311++G(d,p)	Parameters	B3LYP/6-311++G(d,p)
α_{xx}	231.128	β_{xzz}	-5.1214
α_{yy}	163.052	β_{yyy}	-3.5436
α_{zz}	247.793	β_{xxy}	2.2736
α_{Tot}	31.7134×10^{-24} e.s.u	β_{yyz}	2.8320
$\Delta\alpha$	60.4370×10^{-24} e.s.u	β_{zzz}	90.2024
μ_{Tot}	0.3621 Debye	β_{xxz}	3.2548
β_{xxx}	2.1240	β_{yzz}	3.6820
β_{xyy}	-35.7641	β_{Tot}	0.8989×10^{-30} e.s.u.

4.6. Natural bond orbital analysis

The natural bond orbital analysis is a useful method to provide information about the interactions of both filled and virtual orbital spaces. It can enhance the prediction of inter and intra-molecular interactions. The natural bond orbital analysis has been performed by Gaussian 16W program package at the DFT/B3LYP/6-311++G(d,p) method. The electron donor-acceptor overlap orbitals on its stabilization energy E(2) arises from second-order perturbation theory and it can be calculated from the following equation (eqn. 17) [28],

$$E(2) = \frac{q_i\, F(i,j)^2}{\varepsilon_j - \varepsilon_i} \quad (17)$$

where, q_i is the population of donor orbitals; ε_i, ε_j are the diagonal elements of NBO orbitals; $F(i,j)$ is the off-diagonal NBO Fock matrix element between i and j NBO orbitals. Some important interactions between the donor-acceptor NBOs are shown in Table S2 (Supplementary Table 2).

The largest stabilization energy shows that bonding σ (7C–15C) to anti-bonding σ* (4C–20H) orbital having the highest E(2) value of 96.27 kcal/mol. The interaction between σ (1C – 7C) → σ* (9C–10C); σ (2C – 4C) → σ* (4C–20H); σ (7C – 8C) → σ* (9C–10C) stabilizes the molecule with the energy of 49.76, 54.83 and 91.15 kcal/mol respectively. The σ (16C–18O) → σ* (9C–10C) helps the molecule to stabilize with the energy of 62.90 kcal/mol. The interaction between lone pair to anti bonding orbital shows LP (1) 17O → σ* (9C–10C) and σ* (4C–20H) interaction gives stabilization energy of 73.58 and 26.08 kcal/mol respectively. The interaction of LP(1) 18O → σ* (4C–20H) system also enhances the stability by 90.94 kcal/mol. NBO analysis revealed that the π (3C – 5C) → π* (4C – 6C), π (4C – 6C) → π* (13C–14C), π (11C – 12C) → π* (2C – 9C) and π (13C–14C) → π* (11C–12C) interactions give a strong stabilization energy of the title compound by 35.33, 34.37, 36.65 and 17.43 kcal/mol respectively. The presence of other conjugated double bonds and their interactions also enhance the stability further.
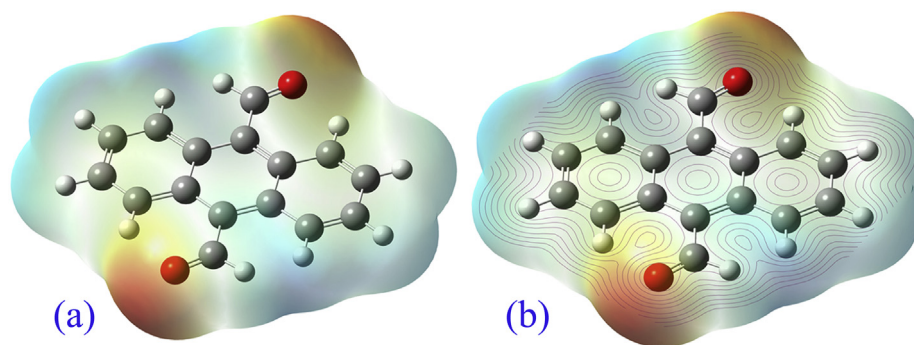
Figure 4. (a) ESP and (b) contour diagram of ADCA.

4.7. Hole electron interaction analysis

The hole-electron analysis module of Multiwfn 3.8 is reasonably very authoritative to analyze all kinds of electron excitations that take place within a molecule. It is useful to analyze the electronic excitation character of a molecule. The molecule under investigation is first optimized by the B3LYP/6-311++G(d,p) basis set. Then time-dependent density functional theory (TDDFT) calculation is carried out for the five lowest singlet excited states. The CAM-B3LYP method is employed with IOp(9/40 = 4) keyword. The.fch file is generated and analyzed. The various results obtained are tabulated in Table 5. The hole-electron distribution, Chole-Celectron function, S_r, and Charge density difference (CDD) functions are shown in Figure 5.

The S_r index values are greater than 0.5 a.u. for all excitations (the theoretical upper limit is 1), which is a larger value, inferring that about half part of hole and electron has perfectly matched. This prediction confirms the presence of a typical local type of excitation (LE). The S_r indices value for the entire excited state is relatively larger. Particularly the excitation from S0 → S4 is rather large up to 0.8547 a.u. The main reason for this higher value is highly localized π-π* type of excitation is present on the aromatic ring. In the other excitations, only n-π* type of excitation is involved.

The H index reflects the breadth of the average distribution of hole and electron. Table 5 gives information about the H index and it is found to be large. Since the distribution of hole and electron corresponding to all the excitations from S0 to S5 are evidently wider, their H indices are evidently larger (Figure 5).

All the τ index values are negative (much less than zero) which means there is no significant separation of hole and electron distributions. This also confirms the absence of charge transfer (CT) type of excitation and insists on the presence of LE type of excitation only.

The hole-electron Coloumb attractive energy is closely related to electron excitation properties. Always D index influences on it. The larger the D index is, the farther the distance between the main distribution regions of hole and electron, and thus the weaker the Coulomb attractive energy. Among all the excitations, S0→S4 is slightly larger (5.2152 eV). From the above results, we can conclude that,

S0 → S1: LE type of excitation with n→π* transition
S0 → S2: LE type of excitation with n→π* transition
S0 → S3: LE type of excitation with n→π* transition
S0 → S4: LE type of excitation with π→π* transition
S0 → S5: LE type of excitation with n→π* transition

According to Kasha's rule, the first excited state (S0 → S1) of a singlet system is usually the critical state to emit fluorescence and hence plays an important role in molecular photo-physics [29].

The percentage of the hole–electron for all the excitation states are investigated and reproduced in Table 6 and shown in Figure 6. From Table 6 and Figure 6, we can easily understand that S0→S1 has more percentage of holes and electrons (97 and 98 respectively).

4.8. Aromaticity determination

The wave function of the title molecule is generated at the B3LYP/6-311G++(d,p) level of theory. Since the title molecule has three fused aromatic ring structure, it is decided to find out the electron conjugation character. The Multicenter bond order and Normalized multicenter bond order are calculated by using Multiwfn 3.8 tool and listed in Table 7, which indicates that the central aromatic ring has weaker electron conjugation character than the boundary rings for the title molecule. Becke's fuzzy atomic space is used to study the aromaticity of different rings of the title molecule.

Aromaticity cannot be observed directly. So several definitions are of aromaticity have been proposed [30]. The aromatic nature of a molecule can be evaluated from its structural, magnetic, and energetic properties [31, 32, 33, 34, 35, 36]. The PDI (Para Delocalization Index), FLU (Fluctuation Index), PLR (Para Linear Response index) and HOMA (Harmonic Oscillator Measure of Aromaticity) values are calculated from Multiwfn 3.8 package and listed in Table 7 for the molecule ADCA. PDI value is just the average of the DIs (Delocalisation Index) between 8C–14C, 10C–12C, 13C–11C for left; 1C–10C, 2C – 8C, 9C – 7C for center and 1C – 6C, 2C – 5C, 4C – 3C for right rings. From the PDI values, it is concluded that the electron delocalization is stronger in boundary rings than the central ring. So it is also evidence that the boundary rings are having stronger aromaticity.

From the FLU values, it is observed that the central ring has higher values than the boundary rings. Hence it is evident that the boundary rings are more typical aromatic system (benzene) and hence possess larger aromaticity than the central ring. The PLR value also validates this conclusion that boundary rings have larger aromaticity than the central ring. Since the HOMA values of boundary rings are larger than the center ring and it also confirms the aromaticity is larger in boundary rings than the middle ring of the target molecule.

4.9. Simulated scanning tunnelling microscope (STM) analysis

Scanning tunnelling microscope is a powerful tool to record the spatial variations of the tunnelling current in the junction between a sharp metallic tip and a conducting probe surface [37]. Simulating scanning tunnelling microscope images for the title molecule and the anthracene molecule are generated and analysed by using Multiwfn 3.8 tool and is shown in Figure 7 (a) and (b) respectively. The local density of states (LDOS) value for the investigated molecule and anthracene are found to be 0.0009 and 0.0003 a.u. respectively at V = - 2V and Z = 2.2 Å. In these maps, the brighter the white, the larger is the LDOS and thus the stronger the tunnelling current (*I*). The Tersoff-Hamann model shows that *I* is positively proportional to LDOS. It can be seen that *I* signal is more prominent over the two boundary six-membered rings than the central ring for ADCA and anthracene molecules.

4.10. Non-covalent interaction analysis

Non-covalent interaction, otherwise called as RDG, which is a powerful tool to understand the non-covalent interaction within a molecule. RDG (eqn.18) is defined as,

$$RDG(r) = \frac{1}{2(3\pi^2)^{1/3}} \frac{|\nabla\rho(r)|}{\rho(r)^{4/3}} \tag{18}$$

When sign(λ_2)ρ (a.u.) is plotted against RDG, some spikes are

Table 5. Various excitation parameters of ADCA.

Excitations	S_m (a.u.)	S_r (a.u.)	D index (Å)	H index (Å)	τ index (Å)	Excitation energy (eV)	Coulomb attractive energy (eV)
S1	0.4845	0.7751	0.000	3.037	-1.974	2.626	5.0374
S2	0.2756	0.5489	0.007	3.246	-2.576	2.935	5.0510
S3	0.2971	0.5748	0.007	3.273	-2.574	3.138	5.0095
S4	0.5698	0.8547	0.001	2.960	-2.222	3.487	5.2152
S5	0.3521	0.6414	0.000	3.036	-1.967	3.692	5.0240
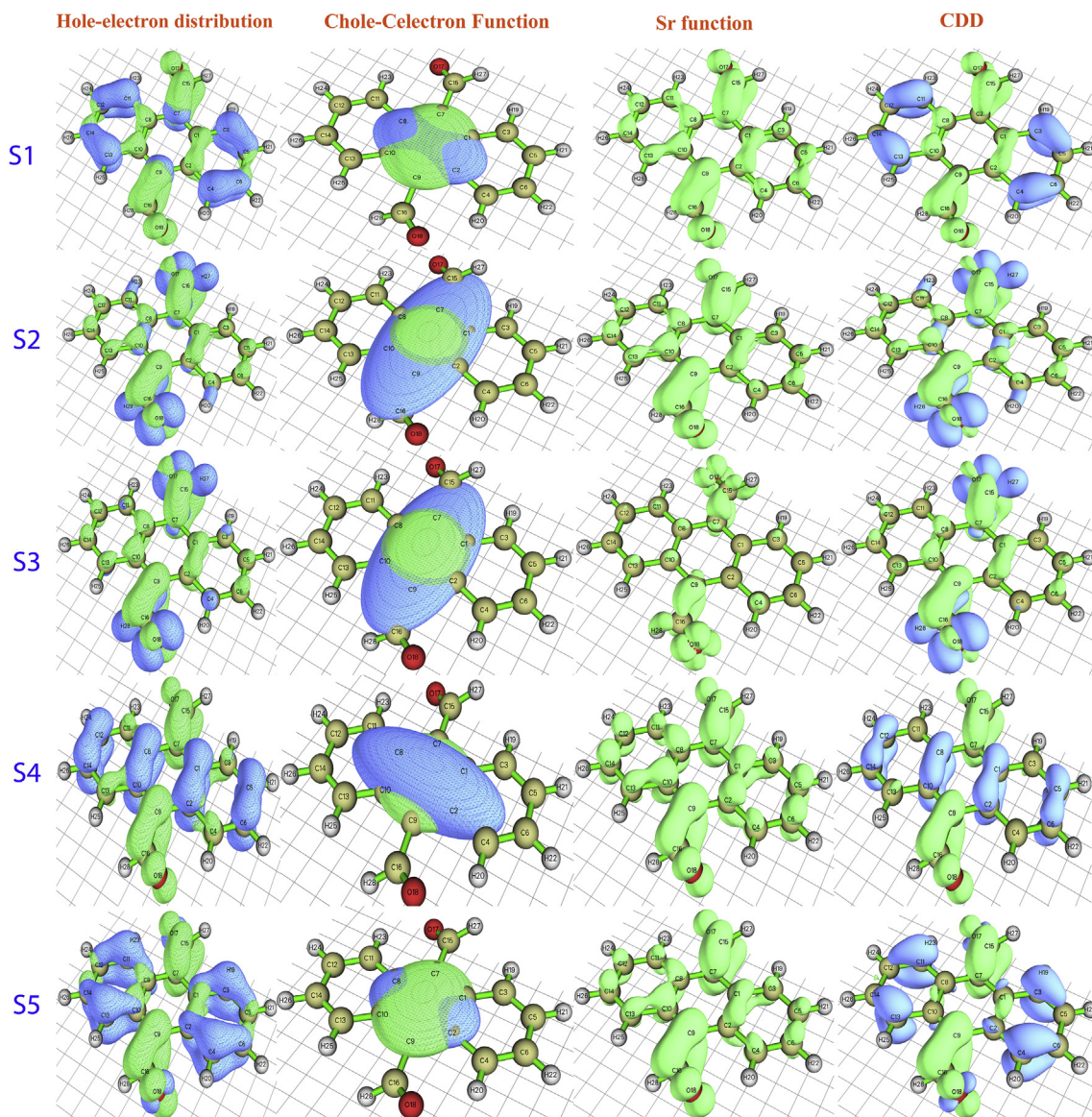
Figure 5. The Hole-Electron distribution, Chole-Celectron function, S$_r$, and CDD representations for all the excitations.

Table 6. Hole-electron percentage involved in various electronic excitations of ADCA.

Excitations	MO	Occupancy	Hole (%)	Electron (%)
S1	61	2.0000	97.265	0.000
	62	0.0000	0.0000	98.490
S2	60	2.0000	82.395	0.000
	62	0.0000	0.0000	94.491
S3	58	2.0000	85.676	0.000
	62	0.0000	0.0000	92.236
S4	59	2.0000	69.376	0.000
	62	0.0000	0.0000	80.311
S5	57	2.0000	86.561	0.000
	62	0.0000	0.0000	96.590

developed. According to the sign(λ_2) and the ρ values, the following regions are defined well.

Strong attraction: halogen bond and hydrogen bond ($\rho > 0$ and $\lambda < 0$).
Van der Waals interaction: ($\rho \approx 0$ and $\lambda \approx 0$).
Strong repulsion: Steric effect in the ring and gage ($\rho > 0$ and $\lambda > 0$).

The NCI (Non-Covalent Interaction) for the title molecule and anthracene are investigated with the help of Multiwfn 3.8 program and the pictures obtained are reported in Figure 8. From Figure 8, it is evident that the target molecule has a steric effect and Van der Waals interactions. The spikes around -0.020 and +0.010 a.u. represents the Van der Waals force of attraction. The spike developed around 0.020 a.u. epitomizes the steric effect present in the ring. In order to prove these facts, two cube files (.cub) are generated by Multiwfn 3.8 and viewed in VMD 1.9.3 tool and the isosurface formed is shown in Figure 8 itself. The brownish green colour spheres represent the presence of Van der Waals force in the molecule and the red spheres in the middle of aromatic rings represent the presence of steric interaction. The same study is carried out for anthracene molecule. In the case of anthracene, the spikes in the negative sign area are missed due to the absence of Van der Waals forces. The spike near +0.020 a.u. is responsible for the steric effect, which is shown as a red sphere in the isosurface of all the aromatic rings.

4.11. Shaded surface map with a projection of LOL investigation

LOL (eqn.19) is a function for locating high localisation regions and it is defined by Schmider and Becke [38, 39].
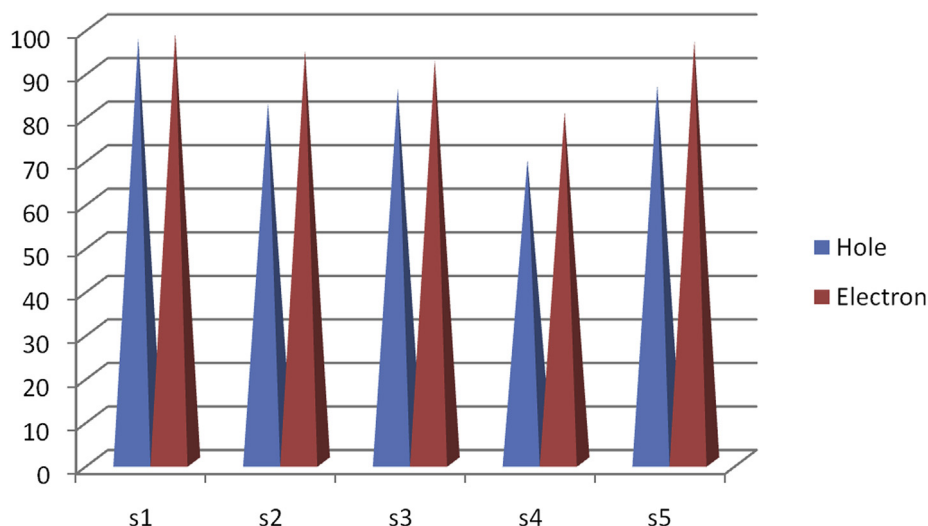
Figure 6. Plot of hole-electron percentage involved in various electronic excitations of ADCA.

Table 7. Various aromaticity parameters of ADCA.

Aromatic ring	Multicenter bond order	Normalized bond order	PDI	FLU	PLR	HOMA
Left	0.0465	0.5996	0.0688	0.0168	0.3821	0.6233
Centre	0.0386	0.5813	0.0549	0.0213	0.3652	0.5673
Right	0.0464	0.5995	0.0688	0.0168	0.3821	0.6233

(a) anthracene-9,10-dicarboxaldehyde   **(b) anthracene**
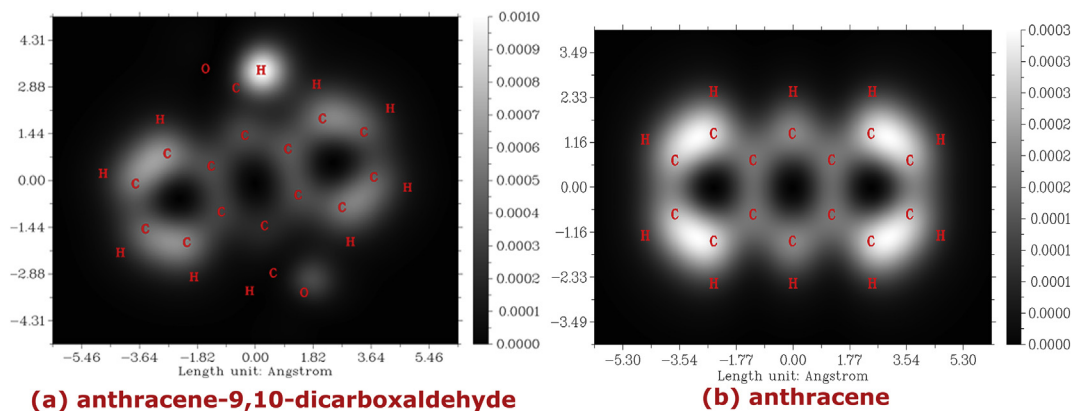
Figure 7. Simulated Scanning Tunnelling Microscope (STM) image of (a) ADCA and (b) anthracene.

$$LOL(r) = \frac{\tau(r)}{1 + \tau(r)} \qquad (19)$$

where the dimensionless variable $\tau(r)$ is $g_0(r)/g(r)$ and always depends on positive one electron kinetic energy density where, $\varphi_i(r)$ are the Hartree – Fock of the Kohn-Sham orbitals. The larger the LOL is in a particular region, the more likely the electron motion is cramped within it. The shaded surface map with a projection of localised orbital locator (LOL) for the title molecule, (ADCA) and anthracene are analysed and the result is evinced in Figure 9 (a) and (b) respectively. In Figure 9, the blue colour in all the carbon atoms represents the depleted electron regions and red colour is related to high localized electron regions. Also, it is evident that all the carbons are having electron depleted area and aromatic hydrogen atoms are having high localized electron regions. It is also evident that the electrons tend to be localised in the outer side of the

rings to stabilise them. Since the backbones of both the rings are same, anthracene also produces similar type of shaded surface map.

4.12. Vibrational studies

4.12.1. Vibrational assignments

Vibrational spectroscopy is the measurement of the interaction between IR radiation and the matter. It is used to study and identify the chemical structure and functional groups in solid, liquid and gaseous forms. The target molecule has 28 atoms in various planes and it undergoes 78 group vibrational modes and finger print vibrations are possible. They are distributed as 28 out of plane vibrations and 50 in-plane vibrations. By adopting DFT/B3LYP/6-311++G(d,p) basis set, the theoretical vibrations are calculated for the title molecule and have been presented in Table 8. The experimental and theoretical IR spectra

(a) anthracene-9,10-dicarboxaldehyde
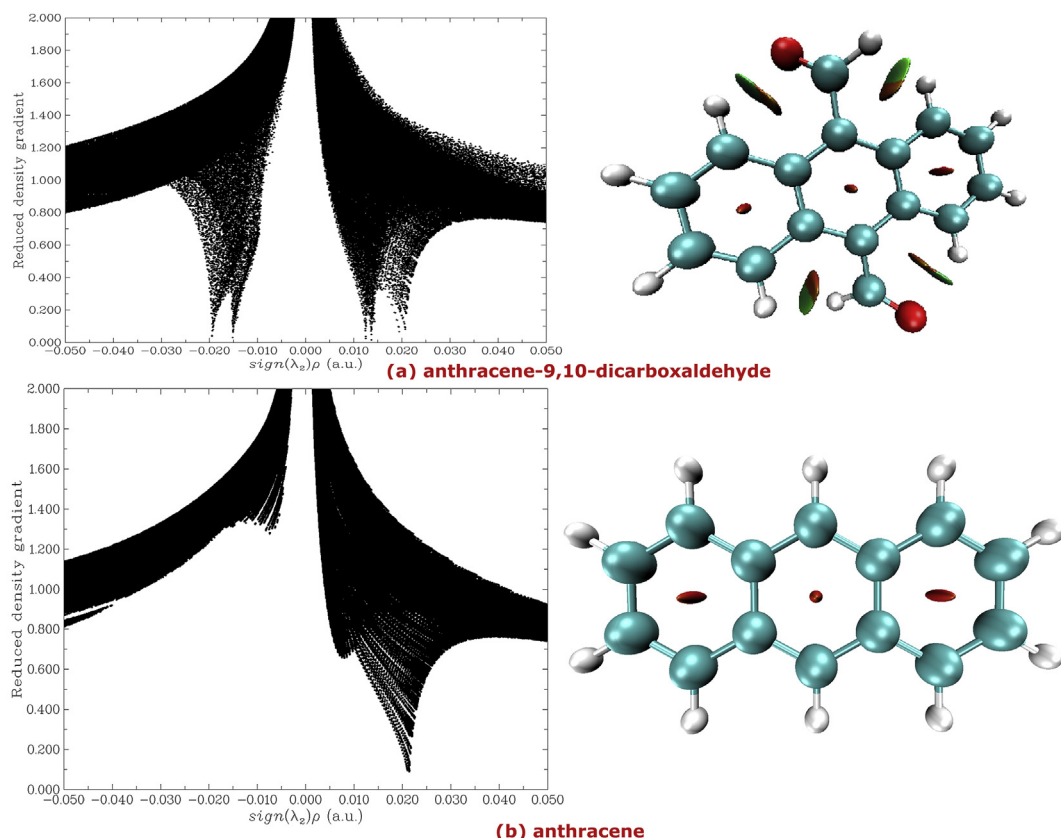
(b) anthracene

Figure 8. The non covalent interaction of (a) ADCA and (b) anthracene.

(a) anthracene-9,10-dicarboxaldehyde
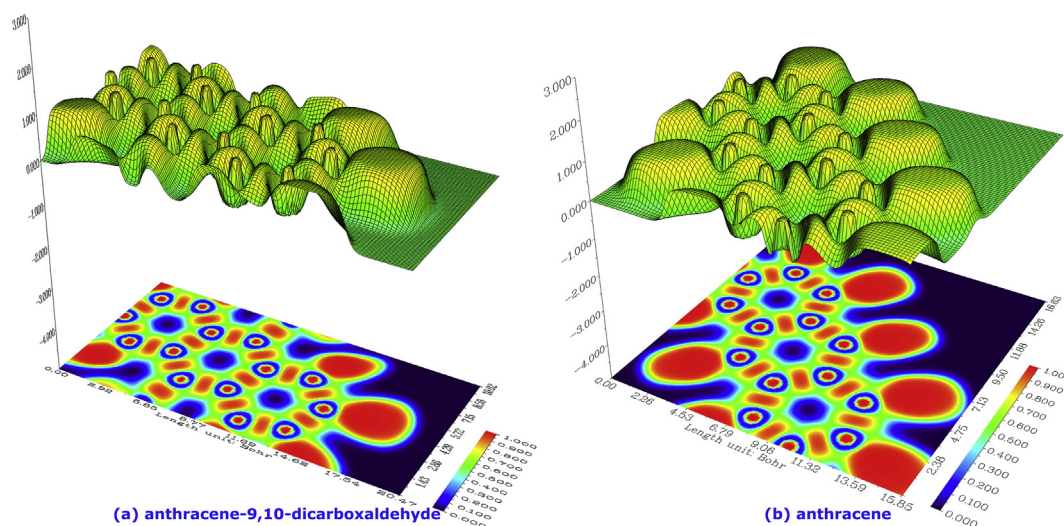
(b) anthracene

Figure 9. Shaded surface map with projection effect of electron localization function (ELF) in the central QM structures of (a) ADCA and (b) anthracene. In this figure, the Z-axis is Localised Orbital Locator (LOL).

are jointly shown in Figure 10 as (A) and (B) respectively. The scaling factor used to calculate the scaled value is 0.967. When compared with the theoretical values, experimental values are found to be lesser. For this study, the results are compared with the work done by Jeyachitra *et.al.,* on 10-methyl anthracene-9-carboxaldehyde and found that the results are in good agreement with them [40].

4.12.2. C–H vibrations

Eight C–H bonds are present in the poly-aromatic anthracene moiety and two hydrogen atoms are attached with the two aldehyde groups. The

C–H stretching vibrations for anthracene can be observed around 3095-2850 cm^{-1} [41]. For the present molecule, the signals at 3154, and 3132 cm^{-1} are allotted to aromatic C–H stretching. The signals at 3081 and 3080 cm^{-1} are fixed to aromatic symmetric C–H stretching while the signal at 3066 cm^{-1} is allotted to aromatic asymmetric C–H stretching. Based on the literature, it is found that the aromatic C–H in-plane bending and out-plane bending modes of vibrations are located in the region 1300-940 cm^{-1} and 1000–720 cm^{-1} respectively [42, 43]. In this investigated molecule, the in-plane bending and out-plane bending modes of vibrations are located at 1514, 1484, 1453, 1427, 1420, 1415,

Table 8. Theoretical and experimental vibrational analysis for the investigated molecule.

SL. NO	Experimental (cm^{-1})	Theoretical (cm^{-1})		Intensity	Assignment of vibrations
		Unscaled	Scaled		
1	3444	3261	3154(w)	19.6876	$\nu(CH)_{aro}$
2	—	3261	3154(w)	11.7990	$\nu(CH)_{aro}$
3	—	3239	3132(vw)	0.1174	$\nu(CH)_{aro}$
4	—	3239	3132(w)	16.7834	$\nu(CH)_{aro}$
5	—	3186	3081(w)	11.1489	$\nu_s(CH)_{aro}$
6	2923	3185	3080(w)	21.5008	$\nu_s(CH)_{aro}$
7	—	3170	3066(w)	3.4093	$\nu_{as}(CH)_{aro}$
8	2853	3170	3066(w)	10.3916	$\nu_{as}(CH)_{aro}$
9	2361	3016	2917(vw)	0.2173	$\nu(CH)_{ald}$
10	1827	3016	2916(S)	125.4329	$\nu(CH)_{ald}$
11	—	1740	1682(vw)	0.0009	$\nu(CO)$
12	1673	1730	1673(VS)	696.2012	$\nu(CO)$
13	—	1665	1610(w)	11.0639	$\nu(CCC)_{aro}$
14	—	1651	1597(vw)	0.0030	$\nu(CCC)_{aro}$
15	—	1589	1537(vw)	0.0018	$\nu(CCC)_{aro}$
16	1527	1573	1521(w)	15.9255	$\nu(CCC)_{aro}$
17	—	1566	1514(vw)	0.0002	$\nu(CCC)_{aro}$, $\delta(CH)_{ald}$
18	—	1535	1484(vw)	0.0000	$\delta(CH)_{aro}$, $\delta(CH)_{ald}$
19	—	1503	1453(w)	18.6415	$\delta(CH)_{aro}$, $\delta(CH)_{ald}$
20	—	1476	1427(w)	24.5438	$\delta(CH)_{aro}$
21	1443	1468	1420(w)	47.7916	$\delta(CH)_{aro}$
22	—	1464	1415(vw)	0.0097	$\delta(CH)_{ald}$, $\delta(CH)_{aro}$
23	—	1419	1372(vw)	0.0002	$\nu(CCC)_{aro}$
24	—	1413	1366(vw)	0.0002	$\delta(CH)_{aro}$
25	1350	1365	1320(m)	91.3256	$\delta(CH)_{aro}$
26	—	1348	1304(m)	56.6941	$\delta(CH)_{aro}$
27	—	1308	1265(vw)	1.0133	$\delta(CH)_{aro}$, $\delta(CH)_{aro}$
28	1279	1291	1249(w)	32.3180	$\delta(CH)_{aro}$, $\delta(CCC)_{aro}$
29	—	1263	1222(vw)	0.0002	$\alpha(CCC)_{aro}$, $\delta(CH)_{aro}$
30	—	1257	1216(vw)	0.0002	$\delta(CH)_{aro}$
31	—	1212	1172(vw)	0.0004	$\delta(CH)_{aro}$
32	1180	1209	1169(w)	36.3148	$\delta(CH)_{aro}$
33	1167	1193	1154(w)	36.1447	$\delta(CH)_{aro}$
34	1114	1131	1094(vw)	0.0001	$\delta(CH)_{aro}$, $\delta(CCC)_{aro}$
35	1022	1072	1036(w)	23.6337	$\delta(CH)_{aro}$
36	—	1070	1035(vw)	0.0011	$\nu(CC)_{ald-aro}$
37	—	1064	1029(vw)	0.0077	$\alpha(CCC)_{aro}$
38	—	1023	989(S)	110.3002	$\delta(CCC)_{aro}$
39	—	1021	988(vw)	0.0063	$\delta(CH)_{aro}$
40	—	1020	987(w)	1.3988	$\gamma(CH)_{aro}$
41	—	995	962(vw)	0.0000	$\gamma(CH)_{aro}$, $\gamma(CH)_{ald}$
42	—	991	959(vw)	0.0383	$\gamma(CH)_{aro}$, $\gamma(CH)_{ald}$
43	—	982	949(vw)	0.6203	$\gamma(CH)_{aro}$, $\gamma(CH)_{ald}$
44	—	979	947(vw)	0.0000	$\gamma(CH)_{aro}$, $\gamma(CH)_{ald}$
45	890	953	922(vw)	0.0000	$\delta(CCC)_{aro}$
46	—	913	883(w)	30.2829	$\delta(CCC)_{aro}$
47	—	868	839(vw)	0.0150	$\gamma(CH)_{aro}$
48	799	867	839(w)	4.0290	$\gamma(CH)_{aro}$
49	—	780	754(vw)	0.0000	$\gamma(CH)_{aro}$
50	—	765	739(vw)	0.0003	$\gamma(CH)_{aro}$
51	—	764	739(S)	116.8936	$\gamma(CCC)_{aro}$
52	745	759	734(S)	101.2938	$\beta(CCC)_{aro}$
53	—	751	726(w)	13.6584	$\beta(CCC)_{aro}$
54	—	748	723(vw)	0.0001	$\gamma(CCC)_{aro}$
55	655	672	650(vw)	0.0000	$\gamma(CCC)_{aro}$
56	—	657	635(w)	14.2354	$\gamma(CCC)_{aro}$
57	593	599	579(w)	28.1706	$\gamma(CCC)_{aro}$

Table 8 (*continued*)

SL. NO	Experimental (cm^{-1})	Theoretical (cm^{-1})		Intensity	Assignment of vibrations
		Unscaled	Scaled		
58	—	593	574(vw)	0.0000	$\gamma(CCC)_{aro}$
59	562	575	556(w)	20.5710	$\gamma(CCC)_{aro}$
60	—	517	500(vw)	0.0000	$\gamma(CCC)_{aro}$
61	—	497	481(vw)	0.1079	$\gamma(CCC)_{aro}$
62	454	475	459(vw)	0.0000	$\gamma(CCC)_{aro}$
63	—	455	440(w)	3.4996	$\gamma(CCCC)$
64	—	425	411(vw)	0.0000	$\gamma(CCCC)$
65	—	411	397(vw)	0.0000	$\gamma(CCCC)$
66	—	389	376(w)	5.8765	$\gamma(CCC)_{aro}$
67	—	344	333(vw)	0.0000	$\gamma(CCC)_{aro}$
68	—	329	318(vw)	0.0000	$\gamma(CCCC)$
69	—	287	277(vw)	0.0002	$\gamma(CCCC)$
70	—	277	268(w)	7.0224	$\gamma(CCCC)$
71	—	271	262(w)	9.7337	$\delta(CH)_{ald}$
72	—	233	225(vw)	0.0000	$\gamma(CCCC)$
73	—	160	155(vw)	0.0238	$\gamma(CH)_{ald}$
74	—	158	152(w)	13.9439	$\gamma(CH)_{ald}$
75	—	126	122(vw)	0.5092	$\gamma(CCCC)$
76	—	67	65(vw)	0.5156	$\gamma(CCCC)$
77	—	56	54(vw)	0.0004	$\gamma(CCCC)$
78	—	18	17(w)	6.5780	$\gamma(CCCC)$

VS – Very Strong; S – Strong; m – medium, w – weak, vw – very weak; s – symmetric; as – Asymmetric; ν - stretching; δ - in plane bending; γ - out plane bending; α - breathing mode; β - Butterfly type; aro – aromatic; ald - aldehyde.

1366, 1265, 1249, 1222, 1216, 1172, 1169, 1154, 1094, 1036 cm^{-1} and 988, 987, 962, 959, 949, 947, 839, 754, 739 cm^{-1} respectively. Some of the in-plane bending vibrations are found well above the expected values may be due to the influence of the two aldehyde groups present in the molecule. The other vibrational signals are located below the expected region. Aromatic C–H butterfly style of vibrations are found at 734 and 726 cm^{-1}. C–H stretching of aldehyde group can be observed at 2917 and 2916 cm^{-1} respectively for both the aldehyde groups. The C–H of aldehyde groups produces signals at 1514 and 1484, 1453 and 1415 cm^{-1} for in-plane bending while their out-plane bending vibrations are located at 962, 959, 949, 947 cm^{-1} as very weak signals.

4.12.3. C=O vibrations

The carbonyl group vibration is always prominence its location between 1750 and 1600 cm^{-1} as a strong intense peak [44]. Two aldehyde groups are attached with the middle aromatic ring of anthracene directly and it is possible to obtain two C=O vibrational peaks. They appear at 1682 and 1673 cm^{-1} in the simulation spectrum. Interestingly the experimental value is also found to be placed exactly on 1673 cm^{-1} as a single strong peak.

4.12.4. C–C vibrations

The poly-nuclear system, anthracene has carbon atoms in its skeleton. They are having some C–C and C=C bonds. The entire C=C and C–C stretching vibrations will be observed in the region 1650–1400 cm^{-1} [40]. In this molecule of interest, the C=C stretching vibrations are located at 1610, 1597, 1537, 1521, 1514, and 1372 cm^{-1}. The C–C stretching vibrations are located at 1320, 1304, 1265, 1249, and 1094 cm^{-1}. The peaks appear in the expected region are in good agreement with the literature which insists the core bond steadiness. The CCC in-plane bending vibrations are observed at 989, 922, 883 cm^{-1} with strong intensities. The CCC out-plane bending vibrations have been seen at 739, 723, 650, 635, 579, 574, 556, 500, 481, 449, 376, 333 cm^{-1}. The middle ring of anthracene molecule breaths at 1222 cm^{-1} and the terminal rings breathe at 1029 cm^{-1}.
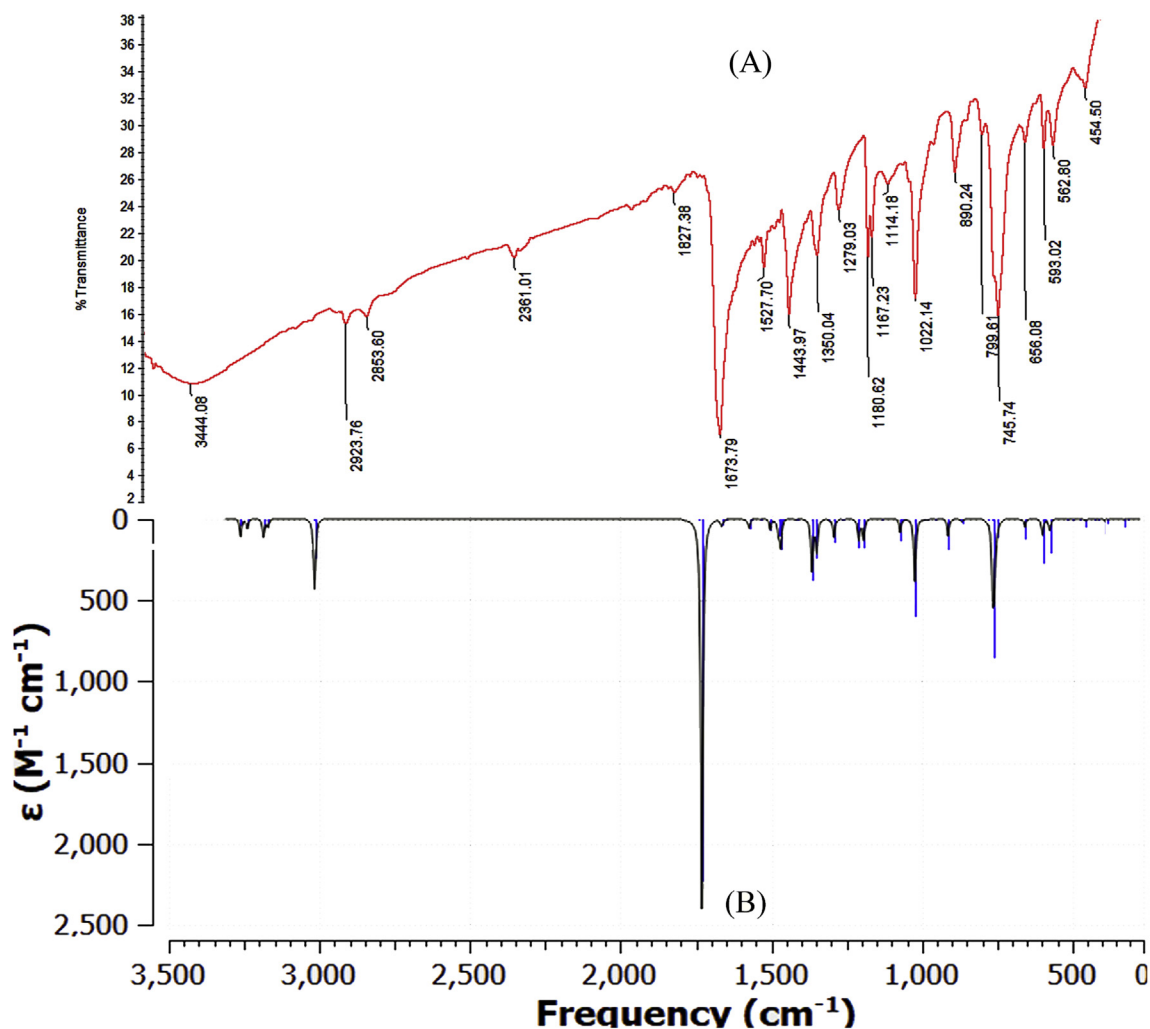
Figure 10. Experimental (A) and simulated (B) IR spectra of ADCA.

4.12.5. CHO vibrations

The aldehyde carbon attached with the nucleus undergoes stretching and is observed at 1035 cm^{-1}. The aldehyde in-plane bending and out-plane bending vibrations are observed at 262, 155, and 152 cm^{-1} respectively.

4.12.6. CCCC and CCCO vibrations

The CCCC and CCCO out plane vibrations for the title molecule are seen at 440, 411, 397, 318, 277, 268, 225, 122, 65, 54, and 17 cm^{-1}.

4.13. UV-visible spectral analysis

The UV Visible spectrum of the target molecule is analysed theoretically from fully optimized ground state structure using ZINDO calculation at the B3LYP/6-311++G(d,p) basis set in ethanol solvent. Experimental UV also has been recorded in ethanol solvent and the two spectra are put together shown in Figure 11. GaussSum 3.0 is used to investigate the other properties like energy, oscillator strength, major contributions and minor contributions etc., and listed in Table 9. Two peaks have appeared for the experimental spectrum (418 and 276 nm) and three spectral values (480, 405, and 398 nm) are obtained for the simulated UV spectrum.

The absorption band appeared at 480 nm in ethanol with molar absorption coefficient (ε) of 20801.85 cm^{-1} arises due to the major electronic transitions from HOMO to LUMO which makes 97%. The absorption band appeared at 405 nm with molar absorption coefficient

(ε) of 24662.01 cm^{-1} arises due to the major electronic transitions from HOMO-4 to LUMO+2 (32%), HOMO-3 to LUMO (40%), while minor transitions include HOMO-3 to LUMO+3 (16%), HOMO-3 to LUMO+6 (2%). Similarly, the peak appeared at 398 nm with molar absorption coefficient (ε) of 25090.29 cm^{-1} arises due to the major electronic transitions from HOMO-4 to LUMO (34%), HOMO-4 to LUMO+3 (18%), HOMO-3 to LUMO+2 (35%), while minor transitions include HOMO-9 to LUMO+2 (3%), HOMO-4 to LUMO+6 (3%) and HOMO-2 to LUMO (2%). The oscillator strengths for the three absorptions are evaluated as 0.4777, 0.0019 and 0.0 respectively.

4.14. Docking studies

4.14.1. In silico prediction of activity spectra for substance (PASS)

The prediction for the activity of anthracene-9,10-dicarboxaldehyde is done with the help of computer programme PASS online server. It predicts the activity spectrum of the compounds as probable activity (Pa) and probable inactivity (Pi). The ratio varies between 0.000 and 1.000. If Pa > 0.7 means, the probability of pharmacological action is high, and if 0.5 < Pa < 0.7, the probability of pharmacological action is less. If Pa is less than 0.5, the compound is unlikely to show pharmacological action [45]. The prediction of activity spectra for substance (PASS) for the target molecule is analysed to find a better choice. From the results obtained, it is decided to carry out docking studies on phobic disorder treatment [Pa < 0.7 (0.849) and Pa> 0.017]. Phobia is a type of anxiety disorder which results in a rapid onset of fear. In Asia, 2-4 % and in Western world 6–8 %
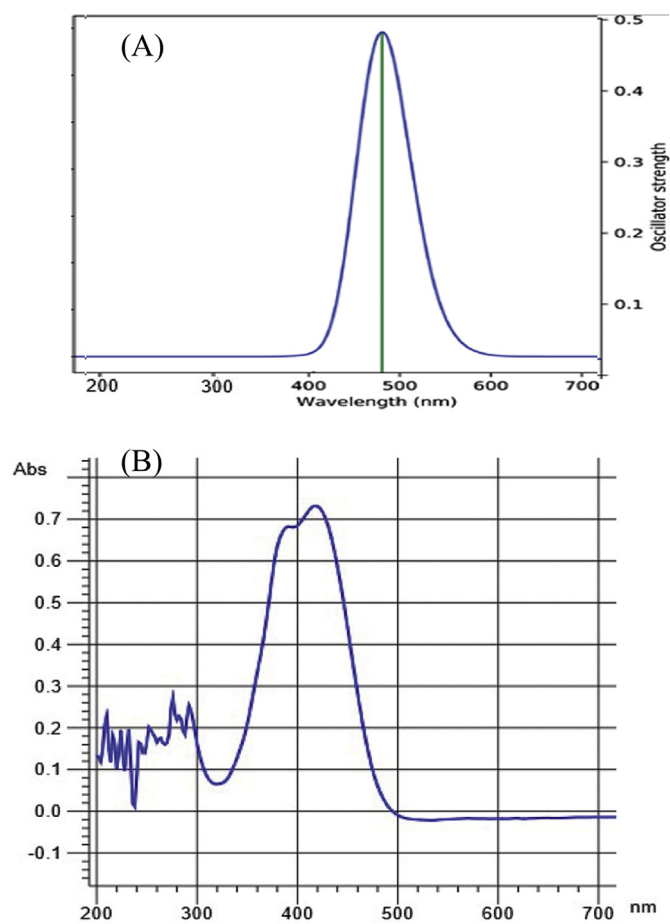
Figure 11. Theoretical (A) and experimental (B) UV – Visible absorption spectra of ADCA.

Table 10. Various properties of the ligand ADCA.

1	Molecular formula	$C_{18}H_{14}O_2$
2	Molecular weight	262.10
3	Number of HBA	2
4	Number of HBD	0
5	MolLogP	4.59
6	MolLogS	-4.56 (in Log(moles/L)) 7.28 (in mg/L)
7	MolPSA	27.35 A^2
8	MolVol	272.35 A^3
9	pKa of most Basic/Acidic group	<0./16.79
10	Number of stereo centers	0
11	nviolations	0
12	nrotb	2
13	Volume	243.12
14	Druglikeness	Yes
15	Lipinski	Yes
16	Ghose	Yes
17	Veber	Yes
18	EGAN	Yes
19	Muegge	Yes
20	Bioavailability score	0.55

Table 11. Docking results and hydrogen bond interaction of ADCA with 4COF.

PDB ID	Ligand	Binding affinity (kcal/mol)	No. of hydrogen bonds developed	H bond distance (Å)	Atom of Ligand	Residue of protein
4COF	ADCA	-6.6	2	2.5	Oxygen	SER-427
				3.2	Oxygen	LEU-294

of people are affected by Phobia. Women are affected by phobias about twice of often as men [46]. Many phobia cases end with suicide. Considering these views, it is decided to carryout research on phobia. So 4COF protein is selected for docking.

4.14.2. Preparation of protein
The X – ray crystal structure of human gamma-aminobutyric acid receptor, GABA(A)R-beta3 homopentamer (PDB ID: 4COF) is retrieved from protein data bank (https://www.rcsb.org/structure/4COF). Before docking, the structure of the protein is prepared by using Discovery Studio 4.1 Visualizer (https://discover.3ds.com/discovery-studio-visualizer-download). Water molecules and the small ligands like hetero-atoms are removed from the protein to make the complex receptor-free of any ligand before docking. Polar hydrogen atoms are added to the protein which is a very essential and crucial step for the computation of partial atomic charges. The force field applied is CHARMm and the partial charge applied is Momany–Rone. Finally, the

protein is subjected to energy minimisation. Ramachandran plot is analyzed for the prepared protein and found that more than 90% of residues fall under the most favoured region.

4.14.3. Preparation of ligand
The 2D structure of the title molecule is drawn with the help of Chemsketch software (https://www.acdlabs.com/resources/freeware/chemsketch/index.php) and saved as .mol file which is then converted to energy minimized 3D structure with the help of Avogadro tool (https://avogadro.cc/) and saved as .pdb. Optimisation of ligand leads to a stable conformation of coordinates with minimum energy. The force field applied is MMFF94 with steepest descend algorithm. The various properties of the ligand are checked for Lipinski's Rule of five from which is presented in Table 10. From that, we could see that the present molecule obeys the rule. SwissADME (http://www.swissadme.ch/) online tool is used to calculate the other properties like bioavailability, drug-likeness etc., and exposed in Table 10. This molecule obeys all the theories and has good drug-likeness property. Also, the bioavailability score is found to be 0.55.

Table 9. Experimental and theoretical electronic absorption spectra of ADCA.

No.	Wavelength (nm) Experimental	Theoretical	Energy (cm^{-1})	Oscillator strength	Major contributions	Minor contributions
1	—	480.7266	20801.85	0.4777	HOMO→ LUMO (97%)	—
2	418.0	405.4819	24662.01	0.0019	H-4→L+2 (32%), H-3→LUMO (40%)	H-3→L+3 (16%) H-3→L+6 (2%)
3	276.0	398.5605	25090.29	0.0	H-4→LUMO (34%), H-4→L+3 (18%), H-3→L+2 (35%)	H-9→L+2 (3%), H-4→L+6 (3%), H-2→LUMO (2%)

Figure 12. The docking pattern of ADCA with the protein 4COF.

4.14.4. Docking

PyRx is a powerful tool that can be used for docking of ligands with proteins. The target molecule is docked with 4COF and the results are analyzed with the help of PyMOL software. Two hydrogen bonds are developed strongly between the ligand and the protein. The docking results are shown in Table 11.

The two oxygen atoms present in the two aldehyde groups of the aromatic rings are bonded with the residues SER-427 and LEU-294 with the hydrogen bond distance of 2.5 and 3.2 Å respectively. The docking score is found to be -6.6 kcal/mol. It clearly suggests that the ligand fits well with the protein, 4COF. The docking pattern viewed by PyMOL is shown in Figure 12.

5. Conclusion

Anthracene-9,10-dicarboxaldehyde is a wonderful molecule with a multinuclear planar system with conjugated double bonds. It has many significant applications in medicinal and industrial fields. The electronic structure and its properties are analyzed theoretically by DFT/B3LYP/6-311++G(d,p) basis set by using Gaussian 16W software. All the bond angle, bond distance and dihedral angles are perfectly matched with the earlier reports well. From the HOMO – LUMO values, it is clear that the molecule is a hard molecule and it is stable. The ESP studies reveal that the molecule is more prone to electrophilic attack near the oxygen atoms of aldehyde groups. NBO study interprets that this is a stable molecule due to high conjugation of double bonds. By using Multiwfn 3.8 tool, the aromaticity of the molecule is determined. It is found that the aromaticity of the central ring is lower than the terminal rings. The STM studies inform that the terminal rings are having more tunneling current than the central ring. The NCI study reveals that the molecule is having steric effect and Van der Waals force of attraction within the molecule. The hole-electron transfer analysis proposes that all the lowest five excitations are of LE type only. Electron depletion area and LOL are determined and interpreted thoroughly for the title molecule through a shaded surface map. IR spectrum is recorded theoretically and experimentally to analyze the various types of vibrations. By using PyRx and PyMOL tools, the docking pattern of the small molecule with 4COF protein is performed and reported.

Declarations

Author contribution statement

J. Jebasingh Kores: Performed the experiments; Analyzed and interpreted the data; Contributed reagents, materials, analysis tools or data; Wrote the paper.

I. Antony Danish: Performed the experiments; Analyzed and interpreted the data; Contributed reagents, materials, analysis tools or data; Wrote the paper.

T. Sasitha: Conceived and designed the experiments; Performed the experiments; Contributed reagents, materials, analysis tools or data; Wrote the paper.

J. Gershom Stuart: Performed the experiments; Contributed reagents, materials, analysis tools or data.

E. Jimla Pushpam: Analyzed and interpreted the data; Contributed reagents, materials, analysis tools or data; Wrote the paper.

J. Winfred Jebaraj: Conceived and designed the experiments; Analyzed and interpreted the data; Contributed reagents, materials, analysis tools or data; Wrote the paper.

Data availability statement

Data included in article/supplementary material/referenced in article.

Declaration of interests statement

The authors declare no conflict of interest.

Additional information

Supplementary content related to this article has been published online at https://doi.org/10.1016/j.heliyon.2021.e08377.

References

[1] R. Ruiterkamp, N.L.J. Cox, M. Spaans, L. Kaper, B.H. Foing, F. Salama, P. Ehrenfreund, PAH charge state distribution and DIB carriers: implications from the line of sight toward HD 147889, Astron. Strophys. 432 (2005) 515–529.

[2] A.V. Kukhta, I.N. Kukhta, N.A. Kukhta, O.L. Neyra, E. Meza, DFT study of the electronic structure of anthracene derivatives in their neutral, anion and cation forms, J. Phys. B Atom. Mol. Opt. Phys. 41 (2008) 205701 (7pp).

[3] H. Okii, H. Hara, Y. Ohba, Electroluminescence in perylene-and-tetracene-doped anthracene films, Jap. J. Appl. Phys. 31 (Part 2 No. 4A) (1992) L416–L418.

[4] D.J. Fatemi, H. Murata, C.D. Merritt, Z.H. Kafafi, Highly fluorescent molecular organic composites for light emitting diodes, Synth. Met. 85 (1997) 1225–1228.

[5] M.X. Yu, J.P. Duan, C.H. Lin, C.H. Cheng, Y.T. Tao, Diaminoanthracene derivatives as high-performance green host electroluminescent materials, Chem. Mater. 14 (2002) 3958–3963.

[6] J.R. Quinn, F.W. Foss Jr., L. Venkataraman, M.S. Hybertsen, R. Breslow, Single-molecule junction conductance through diaminoacenes, J. Am. Chem. Soc. 129 (2007) 6714–6715.

[7] S.E. Adeniji, Density functional theory (DFT) approach for kinetic and thermodynamic study of reaction mechanism of copper(II) complex from 2-hydrazinyl-4,5-dihydro-1h-imidazole and anthracene-9-carbaldehyde, .J. Turk. Chem. Soc. Chem. A 7 (1) (2020) 77–86.

[8] A.D. Becke, Density-functional thermochemistry. III. The role of exact exchange, J. Chem. Phys. 98 (1993) 5648–5652.

[9] C. Lee, W. Yang, R. Parr, Development of the Colle-Salvetti correlation-energy formula into a functional of the electron density, Phys. Rev. B 37 (1988) 785–789.

[10] Gaussian 16, Revision C.01, M.J. Frisch, G.W. Trucks, H.B. Schlegel, G.E. Scuseria, M.A. Robb, J.R. Cheeseman, G. Scalmani, V. Barone, G.A. Petersson, H. Nakatsuji, X. Li, M. Caricato, A.V. Marenich, J. Bloino, B.G. Janesko, R. Gomperts, B. Mennucci, H.P. Hratchian, J.V. Ortiz, A.F. Izmaylov, J.L. Sonnenberg, D. Williams-Young, F. Ding, F. Lipparini, F. Egidi, J. Goings, B. Peng, A. Petrone, T. Henderson, D. Ranasinghe, V.G. Zakrzewski, J. Gao, N. Rega, G. Zheng, W. Liang, M. Hada, M. Ehara, K. Toyota, R. Fukuda, J. Hasegawa, M. Ishida, T. Nakajima, Y. Honda, O. Kitao, H. Nakai, T. Vreven, K. Throssell, J.A. Montgomery Jr.,

J.E. Peralta, F. Ogliaro, M.J. Bearpark, J.J. Heyd, E.N. Brothers, K.N. Kudin, V.N. Staroverov, T.A. Keith, R. Kobayashi, J. Normand, K. Raghavachari, A.P. Rendell, J.C. Burant, S.S. Iyengar, J. Tomasi, M. Cossi, J.M. Millam, M. Klene, C. Adamo, R. Cammi, J.W. Ochterski, R.L. Martin, K. Morokuma, O. Farkas, J.B. Foresman, D.J. Fox, Gaussian, Inc., Wallingford CT, 2016.

[11] J. Trotter, The crystal structure of some anthracene derivatives VI. 9-anthraldehyde, Acta Crystallogr. 12 (1959) 922–928.

[12] P. Pavitha, J. Prashanth, G. Ramu, G. Ramesh, K. Mamatha, B. Venkatram Reddy, Synthesis, structural, spectroscopic, anti-cancer and molecular docking studies on novel 2-[Anthracene-9-ylmethylene)amino]-2-methylpropane-1,3-diol using XRD, FTIR, NMR, UV-Vis spectra and DFT, J. Mol. Struct. 1147 (2017) 406–426.

[13] I.A. Fedorov, Y.N. Zhuravlev, V.P. Berveno, Electronic structure and chemical bond in naphthalene and anthracene, Phys. Chem. Chem. Phys. 13 (13) (2011) 5679–5686.

[14] K.E. Srikanth, K. Ramaiah, D.J. Rao, K.P. Rao, J.L. Naik, A. Veeraiah, J. Prashanth, Experimental and theoretical analyses on structural (monomer and dimeric form), spectroscopic and electronic properties of an organic semiconductor 2,6-dimethoxyanthracene, Indian J. Phys. 94 (8) (2019) 1153–1167.

[15] J.L. Gazquez, Perspectives on the density functional theory of chemical reactivity, J. Mexi. Chem. Soc. 52 (1) (2008) 3–10.

[16] L.I.U. Shu-Bin, Conceptual density functional theory and some recent developments, Acta Phys. Chim. Sin. 25 (3) (2009) 590–600.

[17] P. Geerlings, F. De Proft, W. Langenaeker, Conceptual density functional theory, Chem. Rev. 103 (5) (2003) 1793–1874.

[18] H. Chermette, Chemical reactivity indexes in density functional theory, J. Comput. Chem. 20 (1) (1999) 129–154.

[19] L.H. Mendoza-Huizar, Chemical reactivity of isoproturon, diuron, linuron, and chlorotoluron herbicides in aqueous phase: a theoretical quantum study employing global and local reactivity descriptors, J. Chem. 2015 (2015) 1–9.

[20] P.K. Chattaraj, U. Sarkar, D.R. Roy, Electrophilicity index, Chem. Rev. 106 (6) (2006) 2065–2091.

[21] J.I. Martínez-Araya, G. Salgado-Morán, D. Glossman-Mitnik, Computational nano chemistry report on the oxicams conceptual DFT indices and chemical reactivity, J. Phys. Chem. B 117 (21) (2013) 6339–6351.

[22] C.Y. Panicker, H.T. Varghese, K.R. Ambujakshan, S. Mathew, S. Ganguli, A.K. Nanda, C.V. Alsenoy, J. Raman Spectrosc. 40 (2009) 527–536.

[23] R. Arulraj, S. Sivakumar, S. Suresh, K. Anitha, Synthesis, vibrational spectra, DFT calculations, Hirshfeld surface analysis and molecular docking study of 3-chloro-3-methyl-2,6-diphenylpiperidin-4-one, Spectrochim. Acta Part A Mol. Biomol. Spectrosc. 232 (2020) 118166.

[24] D.A. Kleinmen, Nonlinear dielectric polarization in optical media, Phys. Rev. 126 (1962) 1977–1979.

[25] T. Rajamani, S. Muthu, Electronic absorption, vibrational spectra, non-linear optical properties, NBO analysis and thermodynamic properties of 9-[(2-hydroxyethoxy) methyl] guanine molecule by density functional method, Solid State Sci. 16 (2013) 90–101.

[26] A.E. Reed, L.A. Curtius, F. Weinhold, Intermolecular interactions from a natural bond orbital, donor-acceptor viewpoint, Chem. Soc. 102 (1988) 899–926.

[27] B. Rajasekhar, P.K.M. Hijaz, T. Swu, Computational study on non-linear optical property of wittig based Schiff-base ligands (both Z & E isomers) & copper(II) complex, J. Mol. Struct. 1168 (2018) 212–222.

[28] Z. Demircioglu, A. Kastas, O. Buyukgungor, Theoretical analysis (NBO, NPA, Mulliken Population Method) and molecular orbital studies (hardness, chemical potential, electrophilicity and Fukui function analysis) of (E)-2-((4-hydroxy-2-methylphenylimino)methyl)-3-methoxyphenol, J. Mol. Struct. 1091 (2015) 183–195.

[29] Z. Liu, T. Lu, Q. Chen, An sp-hybridized all-carboatomic ring, cyclo[18]carbon: electronic structure, electronic spectrum, and optical nonlinearity, Carbon 165 (2020) 461–467.

[30] E. Matito, M. Duran, M. Sola`, The aromatic fluctuation index (FLU): a new aromaticity index based on electron delocalization, J. Chem. Phys. 122 (2005), 014109.

[31] T.M. Krygowski, M.K. Cyrański, Structural aspects of aromaticity, Chem. Rev. 101 (2001) 1385–1420.

[32] F. De Proft, P. Geerlings, Conceptual and computational DFT in the study of aromaticity, Chem. Rev. 101 (2001) 1451–1464.

[33] A.R. Katritzky, K. Jug, D.C. Oniciu, Quantitative measures of aromaticity for mono-, Bi-, and tricyclic penta- and hexaatomic heteroaromatic ring systems and their interrelationships, Chem. Rev. 101 (2001) 1421–1450.

[34] J. Gomes, R.B. Mallion, Aromaticity and ring currents, Chem. Rev. 101 (2001), 1349-1349.

[35] M.N. Glukhovtsev, Aromaticity today: energetic and structural criteria, J. Chem. Educ. 74 (1) (1997) 132.

[36] T.M. Krygowski, M.K. Cyrański, Z. Czarnocki, G. Häfelinger, A.R. Katritzky, Aromaticity: a theoretical concept of immense practical importance, Tetrahedron 56 (2000) 1783–1796.

[37] B. Donner, M. Kleber C. Bracher, H.J. Kreuzer, A simple method for simulating scanning tunneling images, Am. J. Phys. 73 (2005) 690–700.

[38] H.L. Schmider, A.D. Becke, Chemical content of the kinetic energy density, J. Mol. Struct. (Theochem) 527 (2000) 51–61.

[39] M.R. Bozorgmehr, J. Chamani, G. Moslehi, Spectroscopic and DFT investigation of interactions between cyclophosphamide and aspirin with lysozyme as binary and ternary systems, J. Biomol. Struct. Dyn. 33 (8) (2015) 1669–1681.

[40] S.M. Beck, D.E. Powers, J.B. Hopkins, R.E. Smalley, Jet-cooled naphthalene. I. Absorption spectra and line profiles, J. Chem. Phys. 73 (1980) 2019–2028.

[41] K. Jayachitra, P.C. JobePrabakar, S. Ramalingam, Vibrational, NMR and UV Visible spectroscopic investigation on 10-methylanthracene-9-carbaldehyde using computational Calculations, J. Mol. Struct. 1217 (2020) 128435.

[42] A.G. Ozkabak, L. Goodman, K. Wiberg, The benzene ground state potential surface. V. Criteria for theoretical modeling of the B2u harmonic force field, J. Chem. Phys. 92 (1990) 4115–4124.

[43] Y. Haas, S. Zilberg, The .nu.14(b2u) mode of benzene in S0 and S1 and the distortive nature of the .pi. Electron system: theory and experiment, J. Am. Chem. Soc. 117 (1995) 5387–5388.

[44] W.R. Ware, B.B. Baldwin, Effect of temperature on fluorescence quantum yields in Solution, J. Chem. Phys. 43 (1965) 1194–1197.

[45] D. Butina, M.D. Segall, K. Frankombe, Predicting ADME properties in silico: methods and models, Drugs Disc. Today 7 (11) (2002) S83–S88.

[46] Diagnostic and Statistical Manual of Mental Disorders, fifth ed., American Psychiatric Publishing, Arlington, 2013, p. 204, 218–219.